BIOCHEMISTRY
including biophysical chemistry & molecular biology
Article

Biochemistry **2011,** *50,* 875–881 875
DOI: 10.1021/bi101717b

Dnmt3a-CD Is Less Susceptible to Bulky Benzo[*a*]pyrene Diol Epoxide-Derived DNA Lesions Than Prokaryotic DNA Methyltransferases[†]

Olga V. Lukashevich,[‡,⊥] Vladimir B. Baskunov,[‡,⊥] Maria V. Darii,[‡,⊥] Alexander Kolbanovskiy,[§] Alexander A. Baykov,[∥] and Elizaveta S. Gromova*[,‡]

[‡]*Chemistry Department, Moscow State University, Moscow 119991, Russia,* [§]*Department of Chemistry, New York University, 31 Washington Place, New York, New York 10003-5180, United States, and* [∥]*A. N. Belozersky Institute of Physico-Chemical Biology, Moscow State University, Moscow 119991, Russia.* [⊥]*These authors contributed equally to this work.*

Received October 25, 2010; Revised Manuscript Received December 21, 2010

ABSTRACT: Benzo[*a*]pyrene (B[*a*]P) is a well-characterized environmental polycyclic aromatic hydrocarbon pollutant. In living organisms, B[*a*]P is metabolized to the genotoxic *anti*-benzo[*a*]pyrene diol epoxide that reacts with cellular DNA to form stereoisomeric *anti*-B[*a*]PDE-N^2-dG adducts. In this study, we explored the effects of adduct stereochemistry and position in double-stranded DNA substrates on the functional characteristics of the catalytic domain of murine de novo DNA methyltransferase Dnmt3a (Dnmt3a-CD). A number of 18-mer duplexes containing site-specifically incorporated (+)- and (-)-*trans-anti*-B[*a*]PDE-N^2-dG lesions located 3′- and 5′-adjacent to and opposite the target cytosine residue were prepared. Dnmt3a-CD binds cooperatively to the DNA duplexes with an up to 5-fold greater affinity compared to that for the undamaged DNA duplexes. Methylation assays showed a 1.7−6.3-fold decrease in the methylation reaction rates for the damaged duplexes. B[*a*]PDE modifications stimulated a nonproductive binding and markedly favored substrate inhibition of Dnmt3a-CD in a manner independent of DNA methylation status. The latter effect was sensitive to the position and stereochemistry of the B[*a*]PDE-N^2-dG adducts. The overall effect of *trans-anti*-B[*a*]PDE-N^2-dG adducts on Dnmt3a-CD was less detrimental than in the case of the prokaryotic methyltransferases we previously investigated.

Benzo[*a*]pyrene (B[*a*]P)[1] is a ubiquitous and harmful pollutant that is abundant in car exhaust and tobacco smoke (*1*) and is metabolically activated to the biologically active benzo[*a*]pyrene-7,8-diol-9,10-epoxides with predominant formation of benzo-[*a*]pyrene-7(*R*),8(*S*)-diol-9(*S*),10(*R*)-epoxide),10(*R*)-epoxide [(+)-*anti*-B[*a*]PDE]. In the *anti* orientation of B[*a*]PDE, the 7-OH and 9,10-epoxide groups are on opposite sites of the planar polycyclic aromatic ring system (*2*, *3*). Both the (+)- and (-)-*anti* enantiomers of B[*a*]PDE bind covalently to the exocyclic amino group of guanine, with *trans* or *cis* opening of the epoxide ring. The most abundant adduct is (+)-*trans-anti*-B[*a*]PDE-N^2-dG, both in vivo (*4*) and in vitro (∼90%) (*5*), with smaller amounts of the (+)-*cis*- and (-)-*trans-anti*-B[*a*]PDE-N^2-dG adduct being formed when native DNA reacts with B[*a*]PDE in vitro (*5*). The B[*a*]PDE-DNA adducts affect the functional properties of a variety of enzymes that include, for example, bacteriophage T7 RNA polymerase (*6*), replicative (*7*) and Y-family DNA polymerases (*8*), HIV-1 integrase (*9*), vaccinia DNA topoisomerase and *Escherichia coli* exonuclease III (*10*), human topoisomerase I (*11*), and human DNA polymerase γ (*12*). Furthermore, B[*a*]PDE-DNA adducts exert significant effects on DNA methylation. The treatment of mouse BALB/3T3 CL1-13 cells with B[*a*]P resulted in a 12% decrease in the overall 5-methylcytosine content of cellular DNA (*13*). Another study showed that exposure of breast cancer cells to B[*a*]P led to dynamic sequence-specific hypo- and hypermethylation events identified in a number of genomic repeats (*14*). The B[*a*]PDE-N^2-dG adducts strongly affect DNA methylation catalyzed by the prokaryotic DNA methyltransferases (MTases), M.SssI, and M.HhaI (*15*, *16*) and fully abolish methylation when located 5′-adjacent to the target cytosine (*15*). High levels of B[*a*]PDE-DNA adducts inhibit DNA methylation by the eukaryotic MTase Dnmt1 (*17*).

The methylation of DNA is an epigenetic modification that plays an important role in the control of gene expression in mammalian cells (*18*). Alterations of the DNA methylation status may constitute a key mechanism in tumorigenesis, because global genomic hypomethylation and gene-specific hypermethylation are observed in nearly all types of tumors (*19*, *20*). DNA methylation in mammals is conducted by three active MTases, Dnmt1, Dnmt3a, and Dnmt3b, using *S*-adenosyl-L-methionine as the methyl group donor. Methylation occurs predominantly at the cytosine residues in CpG sequence contexts, yielding 5-methylcytosines (*21*). Mammalian MTase Dnmt3a is particularly active during embryogenesis and is commonly thought to be responsible for de novo methylation and establishing methylation patterns (*22*). Recently, the role of Dnmt3a in maintenance DNA methylation has been proposed (*23*). It was suggested that the

[†]This research was supported by RFBR Grants 09-04-00869, 10-04-00809, and 08-04-91109/CRDF RUB1-2919-MO-07 and National Cancer Institute Grant CA099194.

*To whom correspondence should be addressed. Telephone: +7 495 939 31 44. Fax: +7 495 939 31 81. E-mail: gromova@genebee.msu.ru.

[1]Abbreviations: AdoHcy, *S*-adenosyl-L-homocysteine; AdoMet, *S*-adenosyl-L-methionine; B[*a*]P, benzo[*a*]pyrene; *anti*-B[*a*]PDE, *r*7,*t*8-dihydroxy-*t*9,10-epoxy-7,8,9,10-tetrahydrobenzo[*a*]pyrene; B^+ and B^-, (+)- and (−)-*trans-anti*-B[*a*]PDE-N^2-dG, respectively; Dnmt3a, DNA methyltransferase Dnmt3a; Dnmt3a-CD, catalytic domain of Dnmt3a; EDTA, disodium ethylenediaminetetraacetate; FAM, 6(5)-carboxyfluorescein; M, 5-methylcytosine; MTase, DNA-(cytosine C5)-methyltransferase.

Published on Web 12/21/2010

bulk of methylation copying is conducted by the maintenance MTase Dnmt1 when DNA is replicated, while Dnmt3a and Dnmt3b complete the methylation process soon after replication and correct errors that are left behind by Dnmt1. Downregulation of Dnmt3a dramatically inhibits the growth and metastasis of malignant melanoma (*24*) and the replication of colorectal cancer cells (*25*). Finally, there are indications that direct Dnmt3a−p53 interactions suppress the p53-mediated transcription of tumor suppressor genes (*26*).

The main objective of this study was to investigate the effects of B[*a*]PDE-induced DNA damage on methylation conducted by the catalytic domain of murine Dnmt3a. We have uncovered the fact that the enzyme can cooperatively bind to B[*a*]PDE-DNA adducts with the formation of nonproductive complexes, in particular, at high adduct concentrations (substrate inhibition). However, there is little effect of lesions on the catalytic constant at low adduct concentrations. Accordingly, we conclude that the overall effects of *trans-anti*-B[*a*]PDE-N^2-dG adducts on Dnmt3a-CD activity are less severe than those associated with prokaryotic methyltransferases.

EXPERIMENTAL PROCEDURES

Chemicals and Buffers. *S*-Adenosyl-L-homocysteine was purchased from Sigma (St. Louis, MO). [CH_3-^{3}H]AdoMet (77 Ci/mmol, 13 μM) was obtained from Amersham Biosciences (Little Chalf-ont, U.K.) and [γ-^{32}P]ATP (1 Ci/μmol) from Isotop (Obninsk, Russia). B[*a*]PDE-modified oligodeoxynucleotides (Table 1) were synthesized as described previously (*15*). Other oligodeoxynucleotides were purchased from Syntol (Moscow, Russia) and IDT (Coralville, IA). The fluorescein label (FAM) was introduced at the 5′-end of the oligodeoxynucleotides using an aminoalkyl linker containing six methylene groups. The oligodeoxynucleotide concentrations were determined spectrophotometrically (*27*).

The following buffers (B1−B7) were used: B1, 50 mM sodium phosphate (pH 6.0), 1 M NaCl, 10 mM mercaptoethanol, 10% (v/v) glycerol, and 0.1% Triton X-100; B2, buffer B1 containing 17 μg/mL phenylmethanesulfonyl chloride, 5 μg/mL leupeptin, and 1 μg/mL pepstatin A; B3, B4, and B5, buffer B2 containing 10, 20, and 150 mM imidazole-HCl, respectively; B6, 20 mM Tris-HCl (pH 7.4), 0.2 mM EDTA, 2 mM dithiothreitol, and 5% (v/v) glycerol; B7, 20 mM HEPES-NaOH (pH 7.0), 100 mM KCl, 1 mM EDTA, and 0.2 mM dithiothreitol.

Enzyme Expression and Purification. The N-terminal His_6 tag fusion catalytic domain of Dnmt3a was expressed in *E. coli* BL21(DE3) cells (Novagen) using the pET28a plasmid containing Dnmt3a-CD as a vector, as described previously (*28*). Cells were grown in LB medium at 32 °C with intensive aeration until an A_{600} of ~0.7 was attained. Protein expression was initiated by the addition of 1 mM isopropyl β-D-thiogalactopyranoside. After 3 h, cells were harvested by centrifugation at 3000*g* for 15 min and disrupted with an MSE Sonifier (Crawley, U.K.) in buffer B2. The cell debris was removed by centrifugation. The supernatant was applied to a Ni-NTA agarose column (BD Biosciences Clontech) equilibrated with B1. After being washed with buffers B2−B4, Dnmt3a-CD was eluted with buffer B5. The eluate was dialyzed overnight against buffer B6; glycerol was added to a final concentration of 50% (v/v) and BSA to a concentration of 200 μg/mL. All protein expression and purification steps were performed at 4 °C. The final preparation of Dnmt3a-CD was > 90% pure, as assessed with 12.5% Laemmli polyacrylamide gel electrophoresis. The Dnmt3a-CD concentration was determined by the Bradford assay and expressed in terms of monomer residues.

Table 1: Oligodeoxynucleotide Sequences[a]

designation	sequence
GCGC	5′GAGCCAAGCGCACTCTGA
GMGC	5′GAGCCAAGMGCACTCTGA
B^-CGC	5′GAGCCAAB^-CGCACTCTGA
B^+CGC	5′GAGCCAAB^+CGCACTCTGA
GCB^-C	5′GAGCCAAGCB^-CACTCTGA
GCB^+C	5′GAGCCAAGCB^+CACTCTGA
GMB^-C	5′GAGCCAAGMB^-CACTCTGA
GMB^+C	5′GAGCCAAGMB^+CACTCTGA
CGCG	5′TCAGAGTGCGCTTGGCTC
CGMG	5′TCAGAGTGMGCTTGGCTC

[a] M, 5-methylcytosine; B^+ and B^-, (+)- and (−)-*trans-anti*-B[*a*]PDE-N^2-dG, respectively.

Scheme 1

$$S \xleftrightarrow{K_{d1}} E_2S \xleftrightarrow{K_{d2}} E_4S$$

Fluorescence Polarization Measurements. Fluorescence polarization was measured using FAM-labeled oligodeoxynucleotide duplexes at 25 °C in 500 μL of buffer B7 employing a Beacon 2000 Fluorescence Polarization System (PanVera), with excitation at 488 nm and emission at 535 nm. Oligodeoxynucleotide duplexes (5 nM) containing the FAM label at the 5′-end of one DNA strand (5′-FAM-TCAGAGTGCGCTTGGCTC or 5′-FAM-TCAGAGTGMGCTTGGCTC) were preincubated with 0.1 mM AdoHcy, and the fluorescence polarization of free DNA (P_0) was measured. Dnmt3a-CD was added in 1−5 μL aliquots of a 8.5 μM stock solution to a final concentration of 325−480 nM, and the polarization value (P) was recorded 2 min after each addition. The titration was continued until the polarization values reached a constant value (P_{max}) corresponding to fully bound duplexes. In all cases, the titration curves were determined in at least two independent trials. The binding data were analyzed in terms of Scheme 1 (*29*), where E_2 and E_4 represent the homodimeric and homotetrameric Dnmt3a-CD molecules, respectively, and S denotes FAM-labeled DNA. The dissociation constants, K_{d1} and K_{d2}, were derived from the binding curves by simultaneous fitting eqs 1−5 with SCIENTIST from MacroMath (St. Louis, MO) to the fluorescence polarization values (P) at different total enzyme concentrations ($[E]_0$):

$$P = P_0 + (P_{max} - P_0)(0.5[E_2S] + [E_4S])/[S]_0 \quad (1)$$

$$[E][S]/[E_2S] = K_{d1} \quad (2)$$

$$[E][E_2S]/[E_4S] = K_{d2} \quad (3)$$

$$[E] + [E_2S] + 2[E_4S] = [E_2]_0 \quad (4)$$

$$[S] + [E_2S] + [E_4S] = [S]_0 \quad (5)$$

$[E_2]$ and $[S]$ represent the free enzyme and substrate concentrations, respectively, while $[S]_0$ is the total FAM-DNA concentration. The fitting procedure took into account the mass balance

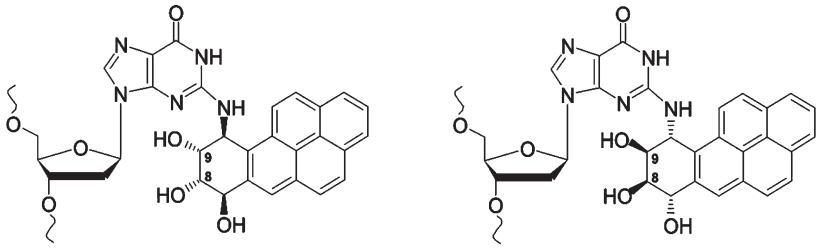

FIGURE 1: Structures of (+) and (−)-*trans-anti*-B[*a*]PDE-N^2-dG adducts.

and the decrease in concentrations of both free enzyme and DNA upon formation of the complex.

Methylation Assays. DNA methylation by Dnmt3a-CD was monitored by measuring the amount of tritium incorporated into the oligodeoxynucleotide duplexes in buffer B7 at 37 °C (*30*). The reaction mixtures contained either 0.1−0.3 μM oligodeoxynucleotide duplex, 1.7−7.6 μM Dnmt3a-CD, and 1.2 μM [CH_3-^{3}H]AdoMet (i.e., the enzyme was in an at least 10-fold excess over substrate) or 2−2.5 μM oligodeoxynucleotide duplex, 0.69 μM Dnmt3a-CD, and 2 μM [CH_3-^{3}H]AdoMet, representing a 2.9−3.6-fold molar excess of a substrate over the enzyme. The reaction was initiated by the addition of [CH_3-^{3}H]AdoMet. After incubation for 4−90 min, 4.9 μL aliquots of the reaction mixtures were pipetted onto DE-81 paper disks (Whatman, Brentford, U.K.). The filters were washed four times with 50 mM KH_2PO_4 and once with water, dried, and placed into 5 mL of ZhS-106 scintillation fluid (Reakhim). The filter-bound radioactivity was measured using a Tracor Analytic Delta 300 scintillation counter (ThermoQuest/CE Instruments, Piscataway, NJ), and the amount of methylated DNA was determined according to a previously described protocol (*30*). The time course of each of the methylation reactions was fit to eq 6

$$[P] = [P]_{lim}(1 - e^{-kt}) \quad (6)$$

where [P] and $[P]_{lim}$ represent the concentrations of methylated DNA at time t and infinity, respectively, and k is the apparent rate constant of methylation.

The initial rate of the methylation reaction (v) was calculated from the relationship $v = k[P]_{lim}$, and the final yield of the methylated product (R) was calculated as $[P]_{lim}/[S]_0$, where $[S]_0$ represents the initial substrate concentration. In experiments measuring only the initial linear parts of the product formation curves, the initial rates of methylation were directly determined from the slopes of these curves, as eq 6 can be approximated by $[P] = kt[P]_{lim}$ in this case.

RESULTS

The aim of this study was to determine whether (+)- and (-)-*trans-anti*-B[*a*]PDE-N^2-dG lesions (hereafter designated B^+ and B^-, respectively) (Figure 1) affect the function of Dnmt3a-CD. We employed the catalytic domain of Dnmt3a, which has a catalytic activity similar to that of the wild-type enzyme (*31*, *32*). Ten different 18-mer oligodeoxynucleotide duplexes with B^+ or B^- incorporated in one strand of the unmethylated or hemimethylated DNA duplexes within or adjacent to the 5′-side of the Dnmt3a-CD recognition sequence were prepared (Table 1). Three families of B[*a*]PDE-damaged duplexes derived from 18-mer undamaged control duplexes GCGC/CGCG, GCGC/CGMG, and GMGC/CGCG were employed in our studies (Table 2). Hemimethylated substrates contained m^5dC instead of target dC either in the strand with damaged guanine (GMGC/CGCG family) or in the complementary strand (GCGC/CGMG family). The methylation rates and catalytic constants obtained under conditions of enzyme or DNA excess, as well as the dissociation constants for these three families of DNA duplexes, are summarized in Table 2.

Effects of B[a]PDE-Derived Lesions on Dnmt3a-CD Binding. Typical binding curves obtained upon titration of the FAM-labeled 18-mer DNA duplexes with Dnmt3a-CD using a fluorescence polarization technique are presented in Figure 2. The binding curves of duplexes not shown in this figure exhibited similar behavior. The cofactor analogue, AdoHcy, was added to mimic the experimental conditions of the methylation assays. The binding curves are clearly sigmoidal in shape for the damaged and undamaged DNA duplexes. These results are consistent with the earlier findings that the interactions of Dnmt3a-CD with undamaged and 8-oxoG-containing 30-mer DNA duplexes are characterized by a positively cooperative mode of binding (*29*).

The curves can be interpreted in terms of Scheme 1, yielding two macroscopic binding constants, K_{d1} and K_{d2} (Table 2), for binding of the two Dnmt3a-CD homodimers to the DNA duplex. As shown in Table 2, K_{d1} exceeded K_{d2} in all cases, whereas a K_{d1}/K_{d2} of 0.25 is expected for noncooperative binding (*33*). The difference between K_{d1} and K_{d2} was particularly large in the case of the GCGC/CGMG duplex and its B[*a*]PDE derivatives, thus making the fraction of the E_2S complex insignificant over the whole range of enzyme concentrations and preventing an evaluation of the magnitudes of the individual binding constants. For these duplexes, only the product $K_{d1}K_{d2}$ could be estimated for comparison with other duplexes.

The binding affinities for B[*a*]PDE-damaged duplexes, characterized by the values of the dissociation constant product $K_{d1}K_{d2}$, were higher than for the corresponding undamaged duplexes in all families (Table 2), except for GCB^+C/CGCG. Notably, the K_{d1} values were more sensitive to the B[*a*]PDE-DNA adducts than the K_{d2} values. This finding is consistent with the mode of binding of Dnmt3a, when the second Dnmt3a dimer is attracted to the DNA molecule by interactions with the first, already bound Dnmt3a dimer, a mechanism that should be less sensitive to the presence of the B[*a*]PDE residues.

Effects of B[a]PDE-Derived Lesions on Dnmt3a-CD Catalysis. The rates of methylation, v_1 and v_2, were measured at two different sets of enzyme and DNA concentrations: enzyme in excess over substrate and substrate in excess over enzyme (Table 2). In the first case, the measurements spanned the complete time course of the reactions (Figure 3), and the time course of the reaction was described well by an exponential function (eq 6). As the extent of substrate conversion was relatively low in the second set of measurements, the product

Table 2: Binding and Kinetic Parameters for Parental and B[*a*]PDE-Damaged DNA Duplexes as Substrates of Dnmt3a-CD

DNA duplex[a]	K_{d1} (nM)	K_{d2} (nM)	$K_{d1}K_{d2}$ (nM^2)	R^b (%)	$v_1{}^c$ (nM/min)	v_2 (nM/min)	$k_{cat,1}{}^d$ (h^{-1})	$k_{cat,2}{}^e$ (h^{-1})
GCGC CGCG	104 ± 26	34 ± 10	3540	95 ± 4	25 ± 4	3.0 ± 0.3	5.2	2.7
B$^-$CGC CGCG	187 ± 54	9 ± 3	1680	94 ± 4	34 ± 6	1.16 ± 0.03	6.9	0.59
B$^+$CGC CGCG	49 ± 12	26 ± 6	1270	100 ± 3	17 ± 1	3.1 ± 0.3	3.4	3.7
GCB$^-$C CGCG	70 ± 25	18 ± 7	1260	70 ± 6	27 ± 6	1.1 ± 0.1	5.5	0.88
GCB$^+$C CGCG	190 ± 59	21 ± 7	3930	74 ± 5	30 ± 7	0.85 ± 0.03	6.2	0.54
GMGC CGCG	170 ± 90	22 ± 6	3720	64 ± 4	12 ± 2	2.6 ± 0.2	2.5	1.8
GMB$^-$C CGCG	73 ± 23	30 ± 11	2190	nd[f]	nd[f]	1.6 ± 0.2	nd[f]	1.7
GMB$^+$C CGCG	80 ± 27	28 ± 13	2130	nd[f]	nd[f]	0.89 ± 0.05	nd[f]	0.92
GCGC CGMG		$K_{d1} \gg K_{d2}$	4400 ± 630	28 ± 4	7 ± 4	2.3 ± 1.3	1.4	0.94
B$^-$CGC CGMG		$K_{d1} \gg K_{d2}$	890 ± 60	13.7 ± 0.3	3.6 ± 0.3	0.36 ± 0.01	0.73	0.14
B$^+$CGC CGMG		$K_{d1} \gg K_{d2}$	1200 ± 190	17 ± 12	3.6 ± 0.8	0.87 ± 0.03	0.73	0.45
GCB$^-$C CGMG		$K_{d1} \gg K_{d2}$	870 ± 120	18 ± 1	5.0 ± 0.6	0.39 ± 0.01	1.0	0.15
GCB$^+$C CGMG		$K_{d1} \gg K_{d2}$	990 ± 80	17 ± 4	3.2 ± 0.6	0.36 ± 0.01	0.65	0.15

[a]The recognition site of Dnmt3a-CD is marked in bold, while the cytosine to be methylated is underlined. [b]Proportion of DNA converted at the end of the reaction in assays conducted when $[E_2]_0 > [S]_0$. [c]The initial rate of methylation measured with 100−300 nM substrate and normalized to 300 nM substrate. [d]Apparent catalytic constant obtained by dividing v_1 by the concentration of the E_4S complex in the corresponding assay. The E_4S concentration was calculated using Scheme 1 with the K_{d1} and K_{d2} values specified in the table. [e]Apparent catalytic constant obtained by dividing v_2 by the concentration of the E_4S complex in the corresponding assay. [f]Not determined.

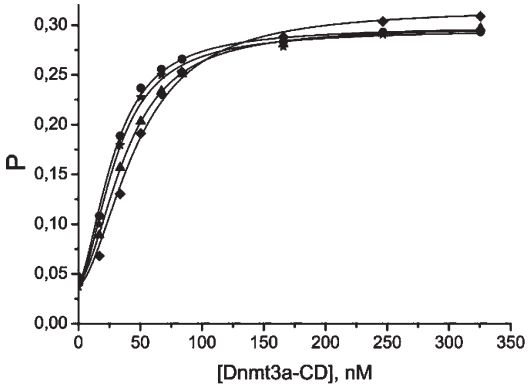

FIGURE 2: Binding curves obtained upon titration of B[*a*]PDE-damaged fluorescein-labeled DNA duplexes (10 nM) with increasing amounts of Dnmt3a-CD in the presence of AdoHcy (0.1 mM). *P* represents the fluorescence polarization value. The total monomeric enzyme concentration is presented. (●) B$^-$CGC/CGMG, (▲) B$^+$CGC/CGMG, (★) GCB$^-$C/CGMG, and (◆) GCB$^+$C/CGMG.

formation curves were linear (Figure 4), allowing for the direct determination of the initial rates of methylation (v_2) from the slopes. The amounts of methylated products accumulating at the end of the incubation period did not exceed the enzyme concentration in either case, which is indicative of single-turnover conditions. It is worth noting that introduction of the B[*a*]PDE residue into DNA had virtually no effect on v_1 values, which were changed by only 1.4−2-fold compared to those for the corresponding undamaged substrates. In contrast, the v_2 values were in most cases decreased by the B[*a*]PDE modifications, by a factor of 1.7−6.3.

The initial rates estimated in the two types of assays (v_1 and v_2 in Table 2) are not directly comparable because the experiments were conducted at different enzyme and substrate concentrations. Therefore, v_1 and v_2 were converted to apparent catalytic rate constants ($k_{cat,1}$ and $k_{cat,2}$, respectively) by dividing these values by the corresponding initial E_4S concentrations. The latter was calculated in each case from the total enzyme and substrate concentrations using the K_{d1} and K_{d2} values determined from the fluorescence titration experiments (Table 2), which was justified by the fact that the FAM label does not affect the DNA−MTase interactions (*27*). In experiments measuring v_1, nearly all the added substrate was present in the form of the E_4S complex, whereas 32−88% of the added enzyme formed E_4S complexes in the experiments designed to determine v_2. The $k_{cat,1}$ and $k_{cat,2}$ estimations were based on the earlier finding that E_4S is the only catalytically competent complex in this system. The E_4S stoichiometry of the substrate complex is consistent with the crystal structure of Dnmt3a-CD in a complex with its orthologous protein Dnmt3L, gel-filtration data, and the results of mutational analysis (*32*, *34*). Furthermore, this stoichiometry is supported by comparison of $P_{max} - P_0$ values for the complexes of GCGC/CGCG with Dnmt3a-CD (0.25−0.26) and M.SssI (0.08−0.09) (data not shown), if one takes into account the fact that the subunit masses of these enzymes are 36 and 44 kDa, respectively, and that M.SssI binds as a monomer. Similar stoichiometries were reported for complexes with 30-mer duplexes (*29*).

The $k_{cat,1}$ values, derived from enzymatic activities measured at low free substrate concentrations, were severalfold lower for the hemimethylated DNA duplexes derived from GMGC/CGCG and GCGC/CGMG than for unmethylated duplexes derived

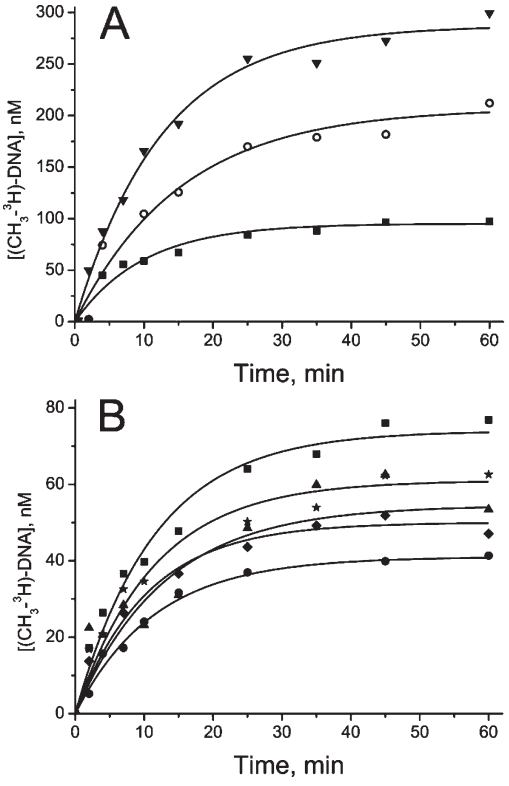

FIGURE 3: Time courses of methylation of selected B[*a*]PDE-damaged (A) and nondamaged (B) DNA duplexes by Dnmt3a-CD with enzyme in excess over DNA. The reaction mixtures contained 300 nM DNA, 5.2−7.6 μM Dnmt3a-CD, and 2 μM [CH_3-^{3}H]AdoMet. (A) GCGC/CGCG (▼), GMGC/CGCG (○), and GCGC/CGMG (■). The symbols in panel B are as specified in the legend of Figure 2.

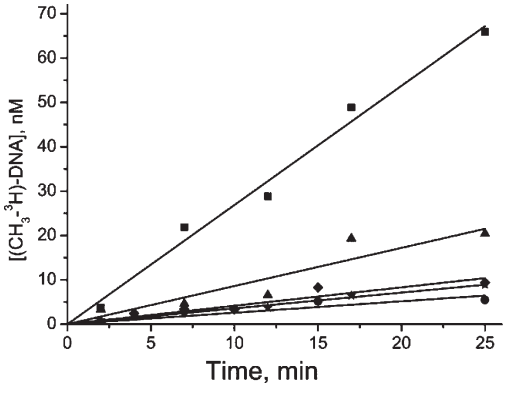

FIGURE 4: Time courses of methylation of selected B[*a*]PDE-damaged duplexes by Dnmt3a-CD with DNA in excess over enzyme. The reaction mixtures contained 2−2.5 μM DNA, 0.69 μM Dnmt3a-CD, and 2 μM [CH_3-^{3}H]AdoMet. Symbols are as specified in the legend of Figure 2.

from GCGC/CGCG but were not significantly affected by the B[*a*]PDE-N^2-dG adducts (Table 2). In contrast, the $k_{cat,2}$ values obtained from the activities measured at high free substrate concentrations displayed more marked variations within each of the three different families of DNA duplexes. In general, B[*a*]PDE-N^2-dG lesions led to a decrease in $k_{cat,2}$ by a factor of 2−7. Furthermore, in most cases, the $k_{cat,2}$ values were lower than the $k_{cat,1}$ values, indicative of substrate inhibition, apparently resulting from nonproductive binding of additional substrate molecule(s) at high substrate concentrations (*33*, *35*, *36*). A difference in the catalytic constants for the damaged substrates varied in the three families of duplexes. The largest difference between $k_{cat,1}$ and $k_{cat,2}$ (up to 12-fold) values was observed with B[*a*]PDE-damaged unmethylated substrates, but no inhibition was evident with one such substrate (B^+CGC/CGCG). Undamaged substrates showed little substrate inhibition, in the unmethylated or hemimethylated form.

Notably, substrate inhibition was negligible at free substrate concentrations of < 10 nM that were used in the $k_{cat,1}$ measurements. Therefore, the $k_{cat,1}$ values refer to the true catalytic constant of Dnmt3a-CD. The differences in $k_{cat,2}$ values mainly reflect the effects of the structure of the substrate on its ability to form a nonproductive complex with Dnmt3a-CD at the higher DNA substrate concentrations.

Formation of Nonproductive Complexes. The final yields (*R*) of methylated products were estimated in assays performed with enzyme in excess. In the case of hemimethylated duplexes, the concentrations of methylated DNA at the end of the reaction were lower than the initial substrate concentrations (0.3 μM) in all cases (Figure 3). On the basis of the results of experiments with other substrate analogues (*29*), these phenomena can be explained in terms of the formation of nonproductive enzyme−substrate complexes. The reaction virtually stops after all of the productive complexes are converted, leaving the substrate intact in the nonproductive complexes, which dissociates very slowly. The *R* value may thus vary from 100% (nonproductive binding does not occur) to 0% (all of the complexes are nonproductive).

For the undamaged, unmethylated substrate (GCGC/CGCG), the *R* value was nearly 100% but decreased significantly in the case of the hemimethylated DNA duplexes (GMGC/CGCG and GCGC/CGMG) (Table 2 and Figure 3A), indicating considerable nonproductive substrate binding. The introduction of B[*a*]PDE-N^2-dG-adducts further decreased the *R* value by approximately 1.5−2-fold (Table 2 and Figure 3B), the effect being somewhat larger in the case of hemimethylated duplexes in which damaged dG was located in the unmethylated strand.

DISCUSSION

Interactions of Dnmt3a-CD with Nondamaged Substrates. As shown previously, two dimeric Dnmt3a-CD molecules bind cooperatively to 30-mer DNA duplexes to form a catalytically competent E_4S complex (*29*). These results suggest that the 18-mer DNA duplexes behave like 30-mer duplexes. Specifically, the sigmoidicity of the binding curves in Figure 2 indicates that two dimeric Dnmt3a-CD molecules bind per DNA duplex and the binding curves exhibit positive cooperativity. The binding affinity is slightly lower; i.e., the $K_{d1}K_{d2}$ value is 4400 nM^2 for the 18-mer GCGC/CGMG duplex (Table 2) versus 830 nM^2 for a 30-mer GCGC/CGMG duplex (*29*). This difference is entirely attributable to the K_{d1} value because K_{d2} values are similar for 18- and 30-mer unmodified duplexes (Table 2 and ref *29*).

On the basis of the *R* values, some inferences about the mode of binding of Dnmt3a-CD to DNA can be made. The yields of the methylated products (*R*) obtained with GCGC/CGCG, GMGC/CGCG, and GCGC/CGMG duplexes as substrates were 95, 64, and 28%, respectively (Table 2). The *R* values of < 100% for the hemimethylated duplexes suggest that the active site is oriented toward the already methylated cytosine in the nonproductive complex of Dnmt3a-CD. This hypothesis is in agreement with the previously published data showing both productive and nonproductive binding of 30-mer hemimethylated duplexes (*29*). The ability of Dnmt3a-CD to bind to the methylated strand stems from the observation that the enzyme can interact with fully

methylated DNA (*29*). That the *R* values are higher for the GMGC/CGCG duplex than for the GCGC/CGMG duplex may indicate preferential binding of Dnmt3a-CD to DNA from the side of the bottom strand (TCAGAGTG**CG**CTTGGCTC and TCAGAGTG**MG**CTTGGCTC, respectively) in both duplexes, consistent with the preferential methylation of the $Py^{-2}Pu^{-1}$**CG**Py^{+1} sequence by Dnmt3a (Py and Pu represent pyrimidine and purine nucleotides, respectively) (*37*, *38*). On this basis, one can further speculate that the flanking sequence has a stronger effect on binding of Dnmt3a-CD to DNA than the methylation status of the target cytosine.

Interestingly, both $k_{cat,1}$ and *R* values for the GMGC/CGCG duplex (2.5 h^{-1} and 64%, respectively) are higher than those for the GCGC/CGMG duplex (1.4 h^{-1} and 28%, respectively). This correlation between the $k_{cat,1}$ and *R* values may mean that the decreased $k_{cat,1}$ value for the latter duplex results solely from an increased level of nonproductive binding. However, more extensive data are needed to further test this hypothesis.

Interactions of Dnmt3a-CD with B[a]PDE-Damaged DNA. The introduction of one B^+ or B^- lesion stimulated the binding of 18-mer DNA duplexes to Dnmt3a-CD (Table 2), as characterized by the K_{d1} and K_{d2} values. The accompanying decrease in *R* suggests that this effect results, at least partly, from nonproductive binding. The increased stabilities of the complexes may result from the contribution of hydrophobic interactions between the B[*a*]PDE residues and the enzyme. The benzo[*a*]pyrenyl moieties are positioned in the minor groove of DNA, oriented toward the 5′- and 3′-ends of the modified strand in the case of the stereoisomeric adducts in the B^+ and B^- duplexes, respectively (*39*, *40*). However, the catalytic constant estimated at low substrate concentrations ($k_{cat,1}$) was only slightly affected by the B[*a*]PDE-N^2-dG adducts.

The major effect of the B[*a*]PDE-N^2-dG lesions is to suppress Dnmt3a-CD activity at high substrate concentrations ($k_{cat,2}$), i.e., to induce strong substrate inhibition. Purdy and co-workers (*41*) recently reported that there was no inhibition of Dnmt3a-CD activity by unmodified DNA substrates. Our data consistently show that substrate inhibition of Dnmt3a-CD by undamaged 18-mer unmethylated and hemimethylated DNA duplexes is quite weak (within the experimental error of $k_{cat,1}$ and $k_{cat,2}$) (Table 2). In contrast, DNA duplexes containing the B[*a*]PDE-N^2-dG adducts, except B^+CGC/CGCG and, possibly, B^+CGC/CGMG, demonstrate strong substrate inhibition of Dnmt3a-CD ($k_{cat,1}/k_{cat,2} \sim 4-12$). For k_{cat} to decrease by a factor of 4−12 at the free substrate concentration of approximately 2 μM, that used in $k_{cat,2}$ measurements, the binding constant describing binding of the inhibiting substrate molecule(s) should be well below 1 μM. The inhibiting substrate molecule(s) may either decrease the true catalytic constant of the productive complex or further decrease the *R* value (i.e., further stimulate nonproductive binding). Notably, the *R* values in Table 2 were derived from assays performed in the absence of substrate inhibition and may not be the same as those of the substrate-inhibited complexes. We cannot distinguish between these alternatives at present because both effects are expected to decrease the observed k_{cat} value. Another corollary is that Scheme 1 is valid only at low substrate concentrations, such as those employed in fluorescence titration experiments and v_1 measurements, and should be supplemented with an E_4S_2 complex at high substrate concentrations.

The stereochemistry of the B[*a*]PDE-N^2-dG adduct does not appear to be important when it is located within the CpG site, because the *R*, $k_{cat,1}$, and $k_{cat,2}$ values are similar for the (+)- and (-)-adduct forms (Table 2). However, the stereochemistry is clearly important when the adduct is located on the 5′-side and adjacent to the target cytosine.

Recent studies have shown that the B[*a*]PDE-N^2-dG-adducts strongly affect DNA methylation catalyzed by the prokaryotic MTases, M.EcoRII, M.HhaI, and M.SssI (*15*, *27*). In fact, methylation by M.HhaI and M.SssI was completely abolished when B^+ or B^- was located on the 5′-side and adjacent to the target cytosine (*15*). Dnmt3a-CD is therefore considerably less sensitive to these adducts because it displays significant methylation activity although at a rate severalfold lower. Moreover, the B[*a*]PDE residues decrease the DNA affinity of M.HhaI up to 100-fold, whereas the same DNA lesions enhance the binding of Dnmt3a-CD to the DNA 4−5-fold. Therefore, we conclude that the methylation activity of Dnmt3a-CD is less affected by the B[*a*]PDE-N^2-dG adducts compared with the prokaryotic MTases. While the evolutionary advantage of such "desensitization" is evident, the elucidation of the underlying mechanism should await determination of three-dimensional structures of the complexes of these enzymes with DNA.

The effects of the B[*a*]PDE-derived lesions on Dnmt3a-CD differ from those of 7,8-dihydro-8-oxoguanine (8-oxoG), another frequently occurring DNA lesion associated with oxidative stress and also with normal cellular metabolism (*42*). Oxidation of guanine to 8-oxoG generates a strong hydrogen bond acceptor at C8 and converts N7 from a proton acceptor to a donor, thus altering the hydrogen bond network between the Dnmt3a-CD and the DNA (*29*). As a result, the binding of hemimethylated DNA duplexes containing 8-oxoG 5′-adjacent to the target cytosine by Dnmt3a-CD is weakened by a factor of 17, and the rate of methylation determined under conditions of DNA excess is decreased by a factor of 4 (*29*). The minor groove B[*a*]PDE-N^2-dG adduct produces similar changes in DNA methylation, and the opposite effect on Dnmt3a-CD binding.

In summary, the B[*a*]PDE-DNA adducts stimulate the binding of Dnmt3a-CD to DNA, enhance the probability of formation of nonproductive complexes, and markedly promote substrate inhibition of Dnmt3a-CD. The latter effect is sensitive to the position and stereochemistry of the adducts. However, the overall effect of B[*a*]PDE on Dnmt3a-CD is less detrimental than it is in the case of prokaryotic methyltransferases.

ACKNOWLEDGMENT

We thank Prof. A. Jeltsch for the Dnmt3a-CD plasmid. We are grateful to Prof. N. E. Geacintov for critically reading the manuscript and helpful discussion.

REFERENCES

1. Phillips, D. H. (1983) Fifty years of benzo(a)pyrene. *Nature 303*, 468–472.
2. Conney, A. H., Chang, R. L., Jerina, D. M., and Wei, S. J. (1994) Studies on the metabolism of benzo[a]pyrene and dose-dependent differences in the mutagenic profile of its ultimate carcinogenic metabolite. *Drug Metab. Rev. 26*, 125–163.
3. Boysen, G., and Hecht, S. S. (2003) Analysis of DNA and protein adducts of benzo[a]pyrene in human tissues using structure-specific methods. *Mutat. Res. 543*, 17–30.
4. Weinstein, I. B., Jeffrey, A. M., Jennette, K. W., Blobstein, S. H., Harvey, R. G., Harris, C., Autrup, H., Kasai, H., and Nakanishi, K. (1976) Benzo(a)pyrene diol epoxides as intermediates in nucleic acid binding in vitro and in vivo. *Science 193*, 592–595.
5. Cheng, S. C., Hilton, B. D., Roman, J. M., and Dipple, A. (1989) DNA adducts from carcinogenic and noncarcinogenic enantiomers of benzo[a]pyrene dihydrodiol epoxide. *Chem. Res. Toxicol. 2*, 334–340.

6. Choi, D. J., Marino-Alessandri, D. J., Geacintov, N. E., and Scicchitano, D. A. (1994) Site-specific benzo[a]pyrene diol epoxide-DNA adducts inhibit transcription elongation by bacteriophage T7 RNA polymerase. *Biochemistry 33*, 780–787.
7. Shibutani, S., Margulis, L. A., Geacintov, N. E., and Grollman, A. P. (1993) Translesional synthesis on a DNA template containing a single stereoisomer of dG-(+)- or dG-(-)-anti-BPDE (7,8-dihydroxy-anti-9,10-epoxy-7,8,9,10-tetrahydrobenzo[a]pyrene). *Biochemistry 32*, 7531–7541.
8. Rechkoblit, O., Zhang, Y., Guo, D., Wang, Z., Amin, S., Krzeminsky, J., Louneva, N., and Geacintov, N. E. (2002) trans-Lesion synthesis past bulky benzo[a]pyrene diol epoxide N2-dG and N6-dA lesions catalyzed by DNA bypass polymerases. *J. Biol. Chem. 277*, 30488–30494.
9. Johnson, A. A., Sayer, J. M., Yagi, H., Patil, S. S., Debart, F., Maier, M. A., Corey, D. R., Vasseur, J. J., Burke, T. R., Jr., Marquez, V. E., Jerina, D. M., and Pommier, Y. (2006) Effect of DNA modifications on DNA processing by HIV-1 integrase and inhibitor binding: role of DNA backbone flexibility and an open catalytic site. *J. Biol. Chem. 281*, 32428–32438.
10. Yakovleva, L., Handy, C. J., Yagi, H., Sayer, J. M., Jerina, D. M., and Shuman, S. (2006) Intercalating polycyclic aromatic hydrocarbon-DNA adducts poison DNA religation by *Vaccinia* topoisomerase and act as roadblocks to digestion by exonuclease III. *Biochemistry 45*, 7644–7653.
11. Pommier, Y., Kohlhagen, G., Laco, G. S., Kroth, H., Sayer, J. M., and Jerina, D. M. (2002) Different effects on human topoisomerase I by minor groove and intercalated deoxyguanosine adducts derived from two polycyclic aromatic hydrocarbon diol epoxides at or near a normal cleavage site. *J. Biol. Chem. 277*, 13666–13672.
12. Graziewicz, M. A., Sayer, J. M., Jerina, D. M., and Copeland, W. C. (2004) Nucleotide incorporation by human DNA polymerase γ opposite benzo[a]pyrene and benzo[c]phenanthrene diol epoxide adducts of deoxyguanosine and deoxyadenosine. *Nucleic Acids Res. 32*, 397–405.
13. Wilson, V. L., and Jones, P. A. (1983) Inhibition of DNA methylation by chemical carcinogens in vitro. *Cell 32*, 239–246.
14. Sadikovic, B., Andrews, J., and Rodenhiser, D. I. (2007) DNA methylation analysis using CpG microarrays is impaired in benzopyrene exposed cells. *Toxicol. Appl. Pharmacol. 225*, 300–309.
15. Subach, O. M., Baskunov, V. B., Darii, M. V., Maltseva, D. V., Alexandrov, D. A., Kirsanova, O. V., Kolbanovskiy, A., Kolbanovskiy, M., Johnson, F., Bonala, R., Geacintov, N. E., and Gromova, E. S. (2006) Impact of benzo[a]pyrene-2′-deoxyguanosine lesions on methylation of DNA by SssI and HhaI DNA methyltransferases. *Biochemistry 45*, 6142–6159.
16. Subach, O. M., Maltseva, D. V., Shastry, A., Kolbanovskiy, A., Klimasauskas, S., Geacintov, N. E., and Gromova, E. S. (2007) The stereochemistry of benzo[a]pyrene-2′-deoxyguanosine adducts affects DNA methylation by SssI and HhaI DNA methyltransferases. *FEBS J. 274*, 2121–2134.
17. Ruchirawat, M., Becker, F. F., and Lapeyre, J. N. (1984) Mechanism of rat liver DNA methyltransferase interaction with anti-benzo-[a]pyrenediol epoxide modified DNA templates. *Biochemistry 23*, 5426–5432.
18. Turek-Plewa, J., and Jagodzinski, P. P. (2005) The role of mammalian DNA methyltransferases in the regulation of gene expression. *Cell. Mol. Biol. Lett. 10*, 631–647.
19. Ehrlich, M. (2002) DNA methylation in cancer: Too much, but also too little. *Oncogene 21*, 5400–5413.
20. Kanai, Y. (2008) Alterations of DNA methylation and clinicopathological diversity of human cancers. *Pathol. Int. 58*, 544–558.
21. Jeltsch, A. (2002) Beyond Watson and Crick: DNA methylation and molecular enzymology of DNA methyltransferases. *ChemBioChem 3*, 274–293.
22. Okano, M., Bell, D. W., Haber, D. A., and Li, E. (1999) DNA methyltransferases Dnmt3a and Dnmt3b are essential for de novo methylation and mammalian development. *Cell 99*, 247–257.
23. Jones, P. A., and Liang, G. (2009) Rethinking how DNA methylation patterns are maintained. *Nat. Rev. Genet. 10*, 805–811.
24. Deng, T., Kuang, Y., Wang, L., Li, J., Wang, Z., and Fei, J. (2009) An essential role for DNA methyltransferase 3a in melanoma tumorigenesis. *Biochem. Biophys. Res. Commun. 387*, 611–616.
25. Ng, E. K., Tsang, W. P., Ng, S. S., Jin, H. C., Yu, J., Li, J. J., Rocken, C., Ebert, M. P., Kwok, T. T., and Sung, J. J. (2009) MicroRNA-143 targets DNA methyltransferases 3A in colorectal cancer. *Br. J. Cancer 101*, 699–706.
26. Wang, Y. A., Kamarova, Y., Shen, K. C., Jiang, Z., Hahn, M. J., Wang, Y., and Brooks, S. C. (2005) DNA methyltransferase-3a interacts with p53 and represses p53-mediated gene expression. *Cancer Biol. Ther. 4*, 1138–1143.
27. Baskunov, V. B., Subach, F. V., Kolbanovskiy, A., Kolbanovskiy, M., Eremin, S. A., Johnson, F., Bonala, R., Geacintov, N. E., and Gromova, E. S. (2005) Effects of benzo[a]pyrene-deoxyguanosine lesions on DNA methylation catalyzed by EcoRII DNA methyltransferase and on DNA cleavage effected by EcoRII restriction endonuclease. *Biochemistry 44*, 1054–1066.
28. Gowher, H., and Jeltsch, A. (2001) Enzymatic properties of recombinant Dnmt3a DNA methyltransferase from mouse: The enzyme modifies DNA in a non-processive manner and also methylates non-CpG [correction of non-CpA] sites. *J. Mol. Biol. 309*, 1201–1208.
29. Maltseva, D. V., Baykov, A. A., Jeltsch, A., and Gromova, E. S. (2009) Impact of 7,8-dihydro-8-oxoguanine on methylation of the CpG site by Dnmt3a. *Biochemistry 48*, 1361–1368.
30. Brennan, C. A., Van Cleve, M. D., and Gumport, R. I. (1986) The effects of base analogue substitutions on the methylation by the EcoRI modification methylase of octadeoxyribonucleotides containing modified EcoRI recognition sequences. *J. Biol. Chem. 261*, 7279–7286.
31. Gowher, H., and Jeltsch, A. (2002) Molecular enzymology of the catalytic domains of the Dnmt3a and Dnmt3b DNA methyltransferases. *J. Biol. Chem. 277*, 20409–20414.
32. Jia, D., Jurkowska, R. Z., Zhang, X., Jeltsch, A., and Cheng, X. (2007) Structure of Dnmt3a bound to Dnmt3L suggests a model for de novo DNA methylation. *Nature 449*, 248–251.
33. Dixon, M., Webb, E. C., Thorne, C. J. R., and Tipton, K. F. (1979) Enzymes, 3rd ed., pp 140−148, Longman Group Ltd., London.
34. Jurkowska, R. Z., Anspach, N., Urbanke, C., Jia, D., Reinhardt, R., Nellen, W., Cheng, X., and Jeltsch, A. (2008) Formation of nucleoprotein filaments by mammalian DNA methyltransferase Dnmt3a in complex with regulator Dnmt3L. *Nucleic Acids Res. 36*, 6656–6663.
35. Segel, I. H. (1993) Enzyme Kinetics: Behavior and Analysis of Rapid Equilibirum and Steady-State Enzyme Systems, John Wiley & Sons, New York.
36. Cornish-Bowden, A. (1995) Fundamentals of Enzyme Kinetics, Portland Press, London.
37. Lin, I. G., Han, L., Taghva, A., O'Brien, L. E., and Hsieh, C. L. (2002) Murine de novo methyltransferase Dnmt3a demonstrates strand asymmetry and site preference in the methylation of DNA in vitro. *Mol. Cell. Biol. 22*, 704–723.
38. Handa, V., and Jeltsch, A. (2005) Profound flanking sequence preference of Dnmt3a and Dnmt3b mammalian DNA methyltransferases shape the human epigenome. *J. Mol. Biol. 348*, 1103–1112.
39. Cosman, M., de los Santos, C., Fiala, R., Hingerty, B. E., Singh, S. B., Ibanez, V., Margulis, L. A., Live, D., Geacintov, N. E., and Broyde, S.; et al. (1992) Solution conformation of the major adduct between the carcinogen (+)-anti-benzo[a]pyrene diol epoxide and DNA. *Proc. Natl. Acad. Sci. U.S.A. 89*, 1914–1918.
40. de los Santos, C., Cosman, M., Hingerty, B. E., Ibanez, V., Margulis, L. A., Geacintov, N. E., Broyde, S., and Patel, D. J. (1992) Influence of benzo[a]pyrene diol epoxide chirality on solution conformations of DNA covalent adducts: The (-)-trans-anti-[BP]G·C adduct structure and comparison with the (+)-trans-anti-[BP]G·C enantiomer. *Biochemistry 31*, 5245–5252.
41. Purdy, M. M., Holz-Schietinger, C., and Reich, N. O. (2010) Identification of a second DNA binding site in human DNA methyltransferase 3A by substrate inhibition and domain deletion. *Arch. Biochem. Biophys. 498*, 13–22.
42. Valko, M., Rhodes, C. J., Moncol, J., Izakovic, M., and Mazur, M. (2006) Free radicals, metals and antioxidants in oxidative stress-induced cancer. *Chem.-Biol. Interact. 160*, 1–40.